The Journal of Experimental Biology 211, 2909-2918
Published by The Company of Biologists 2008
doi:10.1242/jeb.018192

The near and far wake of Pallas' long tongued bat (*Glossophaga soricina*)

L. Christoffer Johansson[1,*], Marta Wolf[1], Rhea von Busse[2], York Winter[2], Geoffrey R. Spedding[3,†] and Anders Hedenström[1]

[1]Department of Theoretical Ecology, Lund University, Sölvegatan 37, SE-223 62 Lund, Sweden, [2]Department of Biology, Bielefeld University, D-33501 Bielefeld, Germany and [3]Department of Aerospace and Mechanical Engineering, University of Southern California, Los Angeles, CA 90098-1191, USA

*Author for correspondence (e-mail: christoffer.johansson@teorekol.lu.se)

†Author's present address: Department of Mechanical and Aeronautical Engineering, University of Pretoria, 0002 Pretoria, South Africa

Accepted 8 July 2008

SUMMARY

The wake structures of a bat in flight have a number of characteristics not associated with any of the bird species studied to this point. Unique features include discrete vortex rings generating negative lift at the end of the upstroke at medium and high speeds, each wing generating its own vortex loop, and a systematic variation in the circulation of the start and stop vortices along the wingspan, with increasing strength towards the wing tips. Here we analyse in further detail some previously published data from quantitative measurements of the wake behind a small bat species flying at speeds ranging from 1.5 to 7 m s^{-1} in a wind tunnel. The data are extended to include both near- and far-wake measurements. The near-/far-wake comparisons show that although the measured peak vorticity of the start and stop vortices decreases with increasing downstream distance from the wing, the total circulation remains approximately constant. As the wake evolves, the diffuse stop vortex shed at the inner wing forms a more concentrated vortex in the far wake. Taken together, the results show that studying the far wake, which has been the standard procedure, nevertheless risks missing details of the wake. Although study of the far wake alone can lead to the misinterpretation of the wake topology, the net, overall circulation of the main wake vortices can be preserved so that approximate momentum balance calculations are not unreasonable within the inevitably large experimental uncertainties.

Supplementary material available online at http://jeb.biologists.org/cgi/content/full/211/18/2909/DC1

Key words: bats, *Glossophaga soricina*, flight, aerodynamics, wake, DPIV.

INTRODUCTION

The wake behind animals may form relatively simple shapes as suggested by numerous bird studies (Hedenström et al., 2006a; Hedenström et al., 2006b; Rosén et al., 2007; Spedding et al., 2003b). On the other hand, the time-varying properties of even fairly simple, three-dimensional model flapping wings can result in very complex pressure distributions on the wing surfaces with a corresponding high complexity of the ensuing wake (Parker et al., 2007; von Ellenrieder et al., 2003). In contrast to the bird wakes, data from bat flight have also shown a rather complex wake pattern [(Hedenström et al., 2007) see also Tian et al. for some preliminary results (Tian et al., 2006)]. The general wake topologies at three different flight speeds (U=1.5, 4 and 6.5 m s^{-1}) have been described by Hedenström and colleagues on the basis of wake velocity and vorticity fields for a small bat species, *Glossophaga soricina* (Hedenström et al., 2007). At the lowest speed studied, 1.5 m s^{-1}, the wings generate a strong start vortex, shed at the trailing edge of the wing at the beginning of the downstroke (Fig. 1) (Hedenström et al., 2007). As the wing stroke progresses, a trailing tip vortex is shed from the wing tip and there is also a companion trailing vortex, of opposite sign to the tip vortex, shed at the wing root, showing that each wing generates its own vortex loop. At the end of the downstroke the wing goes through a pitch-up motion, flipping the wing upside down, which results in the shedding of a distinct combined stop/start vortex for the down- and upstroke (Fig. 1) (Hedenström et al., 2007). The downstroke generates a downward- and somewhat backward-directed jet, for weight support and some thrust to overcome drag. During the upstroke the wing moves backwards relative to the still air with reversed circulation compared with the downstroke, thus also resulting in a backward- and downward-directed jet, for thrust and some weight support. At the end of the upstroke the wing goes through a pitch-down motion, shedding a combined stop/start vortex for the up- and downstroke (Fig. 1) (Hedenström et al., 2007).

At speeds of 4 and 6.5 m s^{-1} a dominant start vortex is generated at the beginning of the downstroke at the outer wing, with trailing patches of start vorticity of lower amplitude, shed throughout the downstroke (Hedenström et al., 2007) (see also Results below). At the inner wing the downstroke is initiated by the wings generating an induced upwash followed by a strong start vortex and trailing patches of start vorticity. As at 1.5 m s^{-1}, both tip and root trailing vortices are found (Fig. 1). When the wing reaches the end of the downstroke the inner wing sheds a diffuse stop vortex. The downstroke generates a downward- and backward-directed jet resulting in weight support and thrust. During the upstroke the wing span is reduced but at the end of the upstroke the wing extends and a weak vortex ring, inducing an upwash (Fig. 1), is visible at the outer wing position (Hedenström et al., 2007) (see also Results below). The inner wing sheds negative-signed vorticity throughout the upstroke, associated with a downwash during the upstroke. The upstroke therefore generates weight support for most of its duration, except at the outer wing towards the end of the upstroke.

The more complicated a wake structure, the more likely it is to twist and bend and deform as it evolves in the wake behind the animal. The deformation as vortex elements are immersed in the

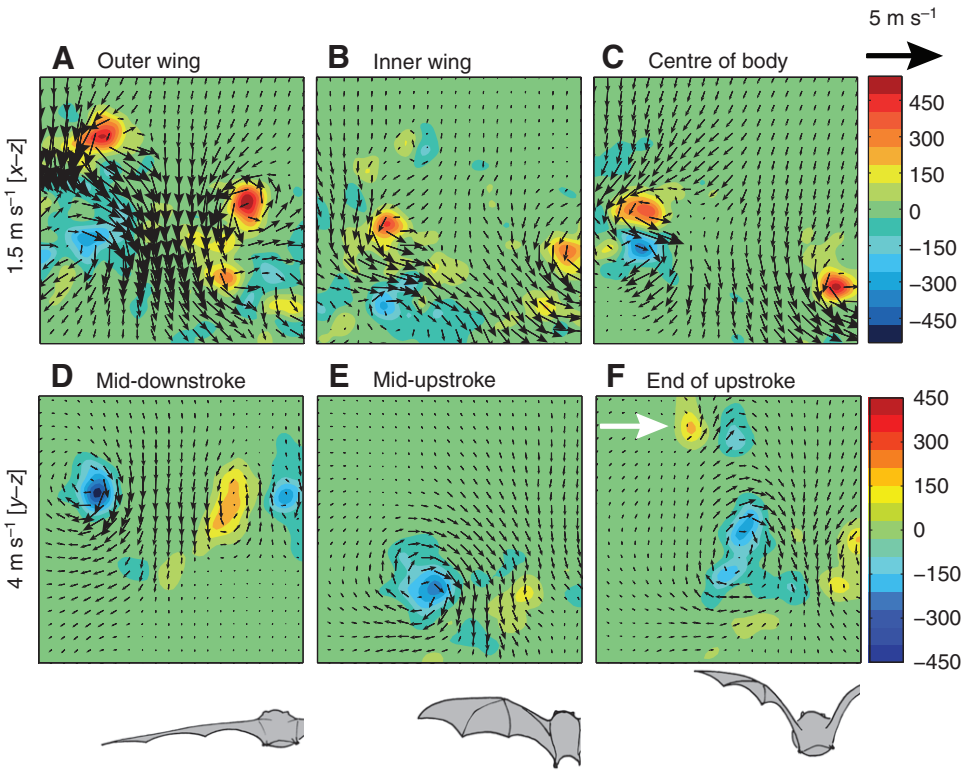

Fig. 1. Wake velocity and vorticity (s^{-1}) plots of the near wake in the streamwise plane [*x*, *z*] for the outer wing (A), inner wing (B) and centre of the body (C) at a flight speed 1.5 m s^{-1}, and in the transverse plane [*y*, *z*] at mid-downstroke (D), mid-upstroke (E) and end of upstroke (F) at a flight speed of 4 m s^{-1}. The white arrow indicates the vortex ring generated at the outer wing during the end of the upstroke. Vorticity is scaled according to the colour bar to the right of each row and vectors are scaled according to the reference vector (modified from Hedenström et al., 2007).

velocity fields induced by themselves and their neighbours is very likely to increase the geometrical complexity. If these deformations are associated with interactions between either like-signed (pairing and merging) or opposite-signed vortices (cancellation) then the topology will also change. Such interactions could arrest the natural development that would have occurred in an otherwise quiet ambient. For example, the roll-up of wingtip vortices that usually occurs within a few chord lengths of the wing trailing edge behind a steady wing may be modified because elements of other smaller scale structures are incorporated too. This kind of effect varies with Reynolds number ($Re=Ul/\nu$, where l is a characteristic length and ν is the kinematic viscosity) in the range of interest to small birds and bats (10×10^4–60×10^4) because the types of vortex shedding on the wing vary with *Re*, and the thickness of the shed structures also varies (e.g. Ramasamy et al., 2007).

In summary, it is likely that the bird or bat wake gradually becomes less and less representative of what the flow near the wing looked like the further downstream it is observed. It is somewhat remarkable that previous measurements of bird wakes, that were made at downstream distances (x) of approximately 15 mean chord lengths (c) behind the wing trailing edge, could be recognized and modelled at all, and it is still possible that these measured structures had deformed significantly from their original shape [see studies by Spedding and colleagues for wake evolution behind steady airfoils at moderate *Re* (Spedding, 2003; Spedding et al., 2006)]. Here we present a more detailed analysis of the bat data than previously (Hedenström et al., 2007), including direct comparisons between near ($x/c>1.1$) and far ($x/c>16$) wake measurements. This will allow us to evaluate the scope and utility of far-wake measurements in animal studies.

MATERIALS AND METHODS

Animals and experimental facility

Two individuals of the tropical species *G. soricina* (Pallas) were used. This bat is nectar feeding and habitually hovers when feeding, suggesting it is well adapted for slow flight (von Helversen, 1986). The bats were weighed before each experimental run and the average body masses are presented in Table 1. The morphometrics of wing planform were measured from in-flight photos using Image J (http://rsb.info.nih.gov/ij/; Table 1), following the procedures of Pennycuick (Pennycuick, 1989) at speed U=5 m s^{-1}.

The bats were trained to fly at a feeder (a metal tube, 2 mm in diameter), providing honey-water, suspended from the ceiling of the Lund University wind tunnel (supplementary material Fig. S1) (Pennycuick et al., 1997). Between feeding bouts the bats roosted on a net 6 m upstream from the test section in the wind tunnel settling chamber. They fed spontaneously by flying downstream into the test section, approaching the feeder *via* a U-turn from the downstream direction. The bats were individually recognized from a video recording showing a rear view. Between experiments, the bats were kept in a room where they could fly freely and had access to fruit, honey-water, Nectar Plus (Nekton, Pforzheim, Germany) and pollen grains *ad libitum*. The temperature in the wind tunnel and roosting facility was kept at 22–27°C and the humidity in the

Table 1. Morphological data

Body mass (kg)	Wing span, *b* (m)	Mean chord, *c* (m)	Wing area (m^2)	AR	Wing loading ($kg\,m^{-2}$)
0.0107±0.00007	0.237	0.037	0.00884	6.4	1.21
0.0109±0.00004	0.243	0.038	0.00936	6.3	1.17

AR, aspect ratio, *b*/*c*.

roosting facility was maintained at >55%. The bats were clock-shifted 12 h so their active (dark) period coincided with lab hours.

Digital particle image velocimetry

The wake measurements were performed using a customized DPIV setup with a double-pulsed laser (Spectra Physics, Quanta Ray PIV II, dual head Nd:YAG, 532 nm; Mountain View, CA, USA) operating at 10 Hz repetition rate. The air was seeded with fog (particle size 1 µm). Pairwise images (separated by δt=200–300 µs) were captured on a CCD array camera (Redlake, Megaplus II ES 4020; Lommel, Belgium) operated in binning mode (1024^2 pixels), and transferred *via* a digital interface (IO Industries, DVR Express 1.23; London, Ontario, Canada) directly to a SCSI disk array (RAID 0) hosted on a PC. To avoid stray light the camera was equipped with an optical bandpass filter of 530±10 nm (Thorlabs, FB 530-10; Göteborg, Sweden). The velocity components u, v and w in the streamwise (x), spanwise (y) and vertical (z) directions were measured in combinations of streamwise [x–z] and spanwise [y–z] imaging planes. The streamwise [x–z] planes were oriented vertically and parallel with the flow downstream of the flying bat at different x and y locations. The spanwise positions are defined as: outer wing (lz), mid-wing (ly), inner wing (lx) and mid-body (lr) (supplementary material Fig. S2). For the near-wake measurements the left edge of the image was 4 cm downstream of the wing trailing edge (or x/c≈1.1) and for the far-wake measurements it was 62 cm downstream of the wing trailing edge (or x/c≈16). Near-wake wing measurements were performed at flight speeds (wind tunnel mean speed, U) ranging from 1.5 to 7 m s^{-1} in 0.5 m s^{-1} increments. Far-wake measurements were performed at flight speeds from 4 to 7 m s^{-1} in 0.5 m s^{-1} increments. At lower speeds the wake had convected too far downwards for the experimental setup. The transverse [y–z] (Trefftz) plane was vertical and spanwise, positioned approximately 12 cm downstream of the wing trailing edge (x/c=3.2), or approximately in the centre of the streamwise images. This setup results in the bat image being faintly visible in the transverse correlation image and so the streamwise distance between the bat and the light sheet was selected to keep the wings of the bat out of phase with the wake. Transverse and near-wake mid-body experiments were performed at three different flight speeds, 1.5, 4 and 6.5 m s^{-1}. Particle image displacements were calculated using correlation image velocimetry (CIV) algorithms (Fincham and Spedding, 1997; Fincham and Delerce, 2000). From the velocity fields we calculated vorticity (ω) in the streamwise plane as:

$$\omega_y = \partial w/\partial x - \partial u/\partial z \,, \quad (1)$$

and in the transverse plane as:

$$\omega_x = \partial v/\partial z - \partial w/\partial y \,. \quad (2)$$

Uncertainty in the estimation of velocity is approximately ±1% and in vorticity is ±10% (Spedding et al., 2003a). Circulation (Γ) was estimated according to Spedding et al. (Spedding et al., 2003b). The circulations for positive (Γ^+, anti-clockwise) and negative (Γ^-, clockwise) patches of vorticity are labelled as 'start' and 'stop' vortices for the streamwise measurements and 'root' and 'tip' vortices for the transverse measurements, respectively. The total circulation of start (Γ_{tot}^+) and stop (Γ_{tot}^-) vortices was also measured in each image by integrating over the entire image. At low speeds, in cases when more than one start or stop vortex was visible in the same image, the strongest vortex core other than the one used for the measurements above was removed from the estimated total circulation in the image.

Kinematics

Two synchronized high-speed cameras (Redlake, MotionScope PCI 500, 250 Hz, 1/1250 s) recorded the bats from side and dorsal views, simultaneously with the DPIV recording during the far-wake experiments. We used infrared illumination (VDI-IR60F, Video Security Inc., Kaohsiung, Taiwan) to avoid disturbing the bats and to minimize interference with the DPIV measurements. The cameras were equipped with infrared filters [Schneider Optics, BW09249 092 (89B); Van Nuys, CA, USA] to eliminate the bright green flashes from the laser. Coordinates of digitized points on the wings

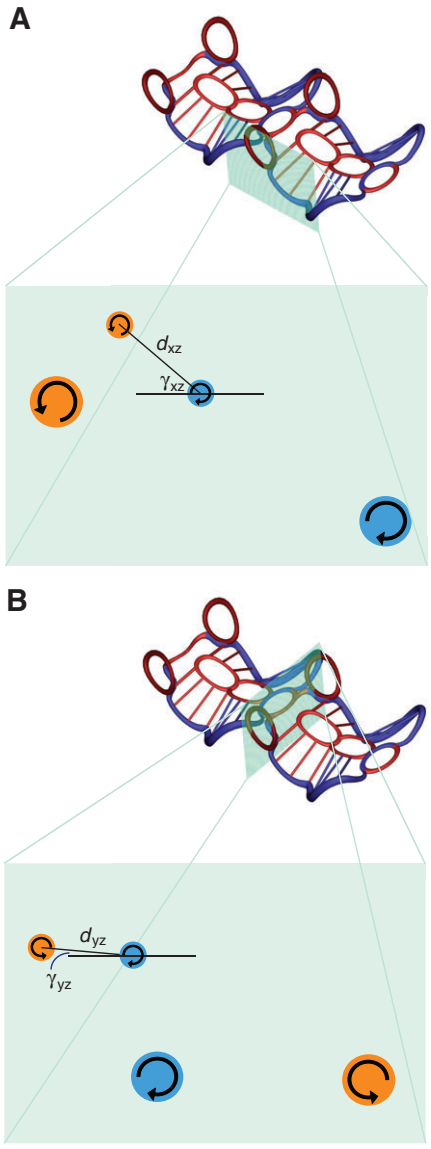

Fig. 2. Definition of the diameter and angle relative to the horizon of the vortex ring generated at the outer wing during the end of the upstroke (see text) as seen in the streamwise [x–z] (A) and transverse [y–z] (B) planes. The small vortices (small orange- and blue-filled circles) represent the outer wing vortex ring. The large circles represent start (orange) and stop (blue) in A and mid-wing vortices in B. The inserted wake models of the near wake at a flight speed of 4 m s^{-1}, as suggested previously (Hedenström et al., 2007), show the laser sheet cut through the wake. Blue cross-stream tubes represent start vorticity and red cross-stream tubes stop vorticity. Blue streamwise tubes represent tip vortices and red streamwise tubes root vortices. At the end of the upstroke the outer wing sheds separate vortex rings, shown in dark red.

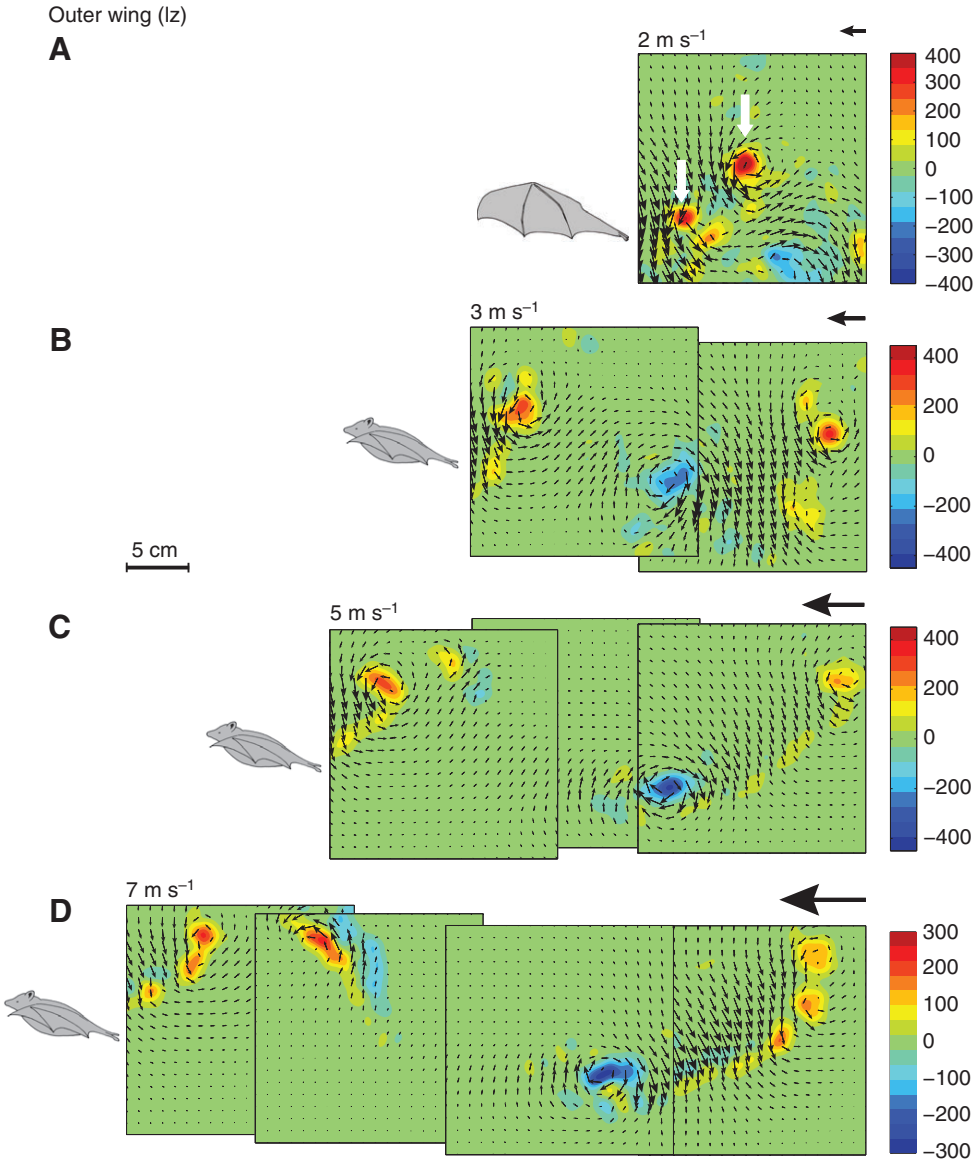

Fig. 3. Composite wake velocity and vorticity (s^{-1}) plots of the near wake in the streamwise plane [*x*, *z*] for the outer wing (lz) at flight speeds of 2, 3, 5 and 7 m s^{-1}. At 2 m s^{-1} the images show double start vortices (white arrows) and a single stop vortex. Vorticity is scaled according to the colour bar to the right of each image and vectors are scaled according to the reference vectors, representing the flight velocity, plotted above each composite plot. The size of the images is indicated by the 5 cm scale bar to the left. The upwash during the upstroke is due to the laser sheet cutting outside the tip vortex.

and body of the bats from the two views were transformed into three-dimensional coordinates by direct linear transformation (DLT), using freely available Matlab® routines (courtesy of Christoph Reinschmidt, http://isbweb.org/software/movanal.html). Based on the movements of these points, wingbeat frequency (*f*) and amplitude (*A*) were calculated (a detailed analysis of the kinematics will be presented elsewhere; M.W., L.C.J., A.H., R.v.B. and Y.W., unpublished data).

Force estimates

In the previous analysis (Hedenström et al., 2007), a vortex dipole with an upward-directed induced flow was observed at the end of the upstroke (eu) at speeds equal to and above 3 m s^{-1}. The vertical contribution of this negative lift was calculated from the circulation of the negative vortex core (Γ_{eu}^{-}) in the streamwise plane [*x*–*z*] of the near-wake vorticity fields. Furthermore, the streamwise diameter (d_{xz}, the distance between the centres of peak positive and negative vorticity) and angle relative to the horizon (γ_{xz}) were measured for speeds from 4 and 6.5 m s^{-1} (Fig. 2A). The diameter (d_{yz}) and angle relative to the horizon (γ_{yz}) were also measured in the transverse plane [*y*–*z*] (Fig. 2B) at the two available speeds (4 and 6.5 m s^{-1}). The negative vertical force (F_v) generated by this vortex dipole was then calculated from the impulse (I_{eu}) according to:

$$F_v = I_{eu}/T_{eu} = \Gamma_{eu}^{-}\rho S_{eu}/T_{eu}\,, \quad (3)$$

where ρ is the air density, T_{eu} is the formation time and assuming an ellipsoidal, horizontally projected area of the vortex ring, S_{eu}:

$$S_{eu} = \pi d_{xz}\cos(\gamma_{xz}) d_{yz}\cos(\gamma_{yz})\,. \quad (4)$$

The formation time, the time it takes to generate the vortex ring, was estimated as the horizontally projected length of the vortex ring in the flight direction divided by the forward flight speed as:

$$T_{eu} = d_{xz}\cos(\gamma_{xz})/U\,. \quad (5)$$

Statistics

Before the analysis the dependent variables and the covariate were $\log_e$-transformed to remove non-linearity of the data (see below) and skewness in the distribution (Grafen and Hails, 2002). The mean values for the measurements at each combination of conditions were used as the independent data points, which were weighted using the inverse of the standard error of the mean (s.e.m.). The number of data points for each of the factors is presented in the supplementary

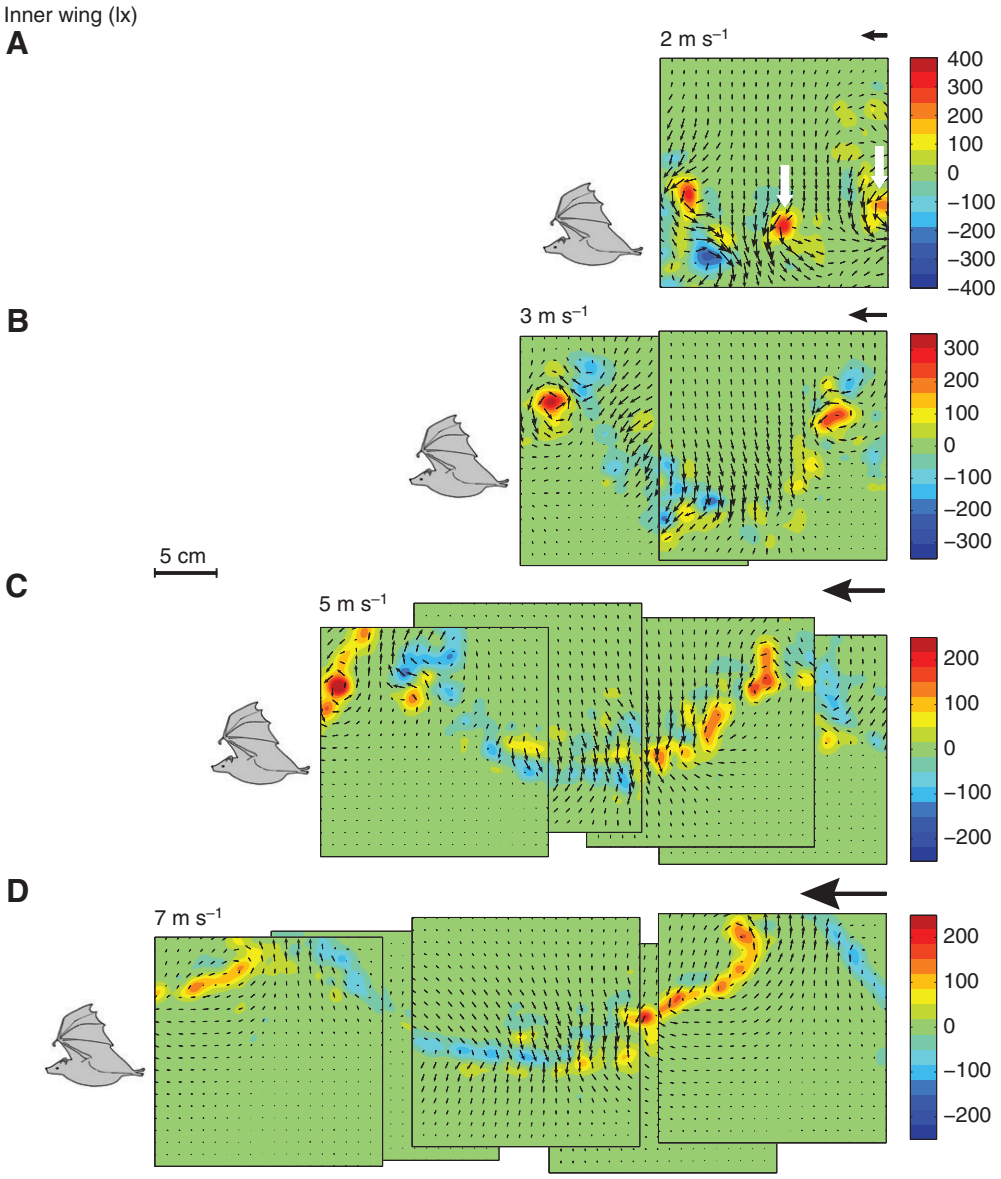

Fig. 4. Composite wake velocity and vorticity plots of the near wake in the streamwise plane [*x*, *z*] for the inner wing (lx) at flight speeds of 2, 3, 5 and 7 m s^{-1}. At 2 m s^{-1} the images show double start vortices (white arrows) and a single stop vortex. For further explanation, see Fig. 3.

material as are the resulting degrees of freedom for each test (supplementary material Tables S1–S7). All analyses were performed using SPSS 15.0 (SPSS Inc., Chicago, IL, USA) with significance level set at 0.05.

We tested for the effect of wing position and sense of circulation (start or stop) on the near-wake streamwise data using a general linear model (GLM) with normalized peak vorticity ($|\omega|c/U$), normalized circulation of the main start or stop vortex ($|\Gamma|/Uc$), normalized total positive or negative circulation in the vorticity field ($|\Gamma_{tot}|/Uc$), or the relative contribution of the main start or stop vortex to the total circulation of start or stop vortices (Γ/Γ_{tot}) as dependent variables. The model was constructed using individual as a random factor and sense of circulation (start or stop) and wing position (lz, ly, lx or lr) as fixed factors. Flight speed was used as a covariate and the model included all main effects and all second-order interactions between factors. Using a linear model on $\log_e$-transformed data is equivalent to modelling the raw data using a power function. This is reasonable since $|\Gamma|/Uc$ is expected to be proportional to U^{-2} (Rosén et al., 2007). The same holds for $|\omega|c/U$, which is proportional to $|\Gamma|/Uc$ (Pearson correlation=0.988).

Differences between near and far wake were determined using the far-wake data and a subset of the near-wake data covering the same speed range. For this test a GLM with the same variables as in the near-wake-only analysis was performed but including wake position (near or far) as a fixed factor.

Differences between the wing tip and wing root vortices in the transverse data were determined using a GLM with normalized peak vorticity ($|\omega|c/U$) or circulation ($|\Gamma|/Uc$) of the vortices as dependent variables. Flight speed was set as covariate, vortex type (tip or root) and stroke phase (mid-downstroke, mid-upstroke and beginning of downstroke) as fixed factors and individual as a random factor.

SPSS calculates estimated marginal means (EMMs), which are the model estimates at the mean value of the covariate for the different factors in the model. The EMMs help to illustrate some of the results.

RESULTS

Wake topology

The general wake topologies at three flight speeds: 1.5, 4 and 6.5 m s^{-1} have been described previously (Hedenström et al., 2007). Composite streamwise [*x*, *z*] velocity fields for the near wake at 2,

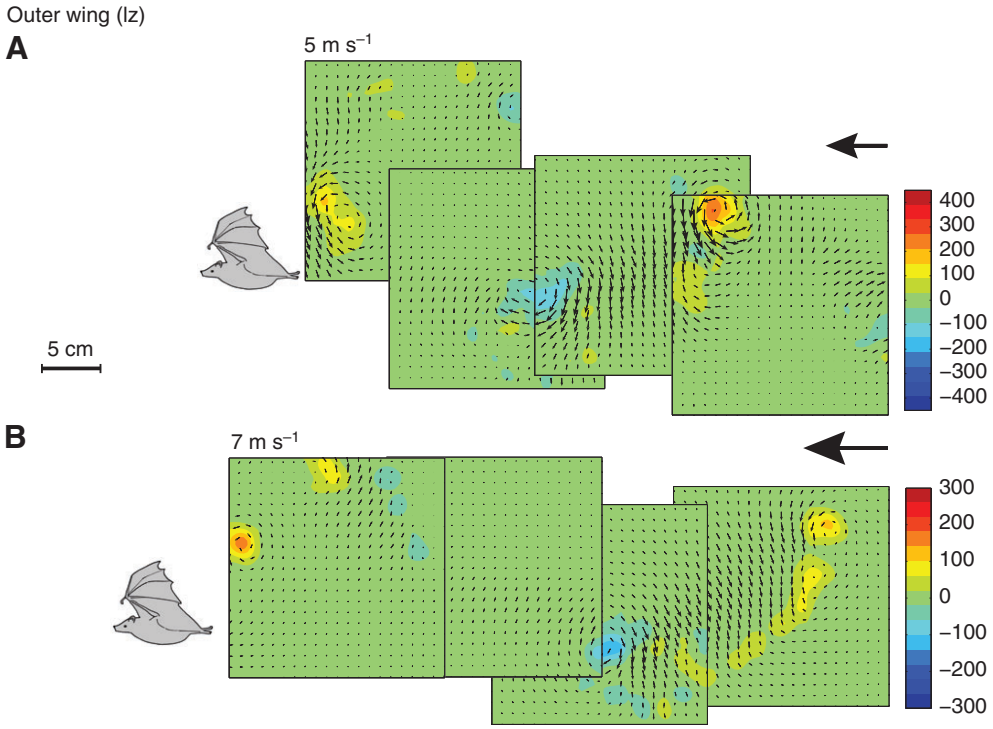

Fig. 5. Composite wake velocity and vorticity plots of the far wake in the streamwise plane [*x*, *z*] for the outer wing (lz) at flight speeds of 5 and 7 m s^{-1}. For further explanation, see Fig. 3.

3, 5 and 7 m s^{-1} and for the far wake at 5 and 7 m s^{-1} for the outer (lz) and inner wing (lx) positions are given in Figs 3–6, selected to complement previously published wakes. In the following section we will emphasize certain characteristics and point out previously undescribed features of the wake.

At U=2 m s^{-1} the wing motion was similar to that at 1.5 m s^{-1} (see above), but the upstroke was more vertical relative to still air than at 1.5 m s^{-1}. The wake in the streamwise plane [*x*, *z*] contained two start vortices and only one stop vortex, a pattern found both at the inner (Fig. 4) and at the outer wing positions (Fig. 3). This pattern was also found at 2.5 m s^{-1} for one of the bats, while the other bat displayed the same wake pattern as at 3 m s^{-1} (see below). At low speeds (1.5–2.5 m s^{-1}) the start and stop vortices in the wake were distinct (Figs 1, 3 and 4), and in contrast to the higher speeds the stop vortex was also distinct at the inner wing position.

For U=3–7 m s^{-1} the wake followed the same qualitative pattern as described by Hedenström and colleagues (Hedenström et al., 2007) for speeds of 4 and 6.5 m s^{-1} (see above). At the inner wing

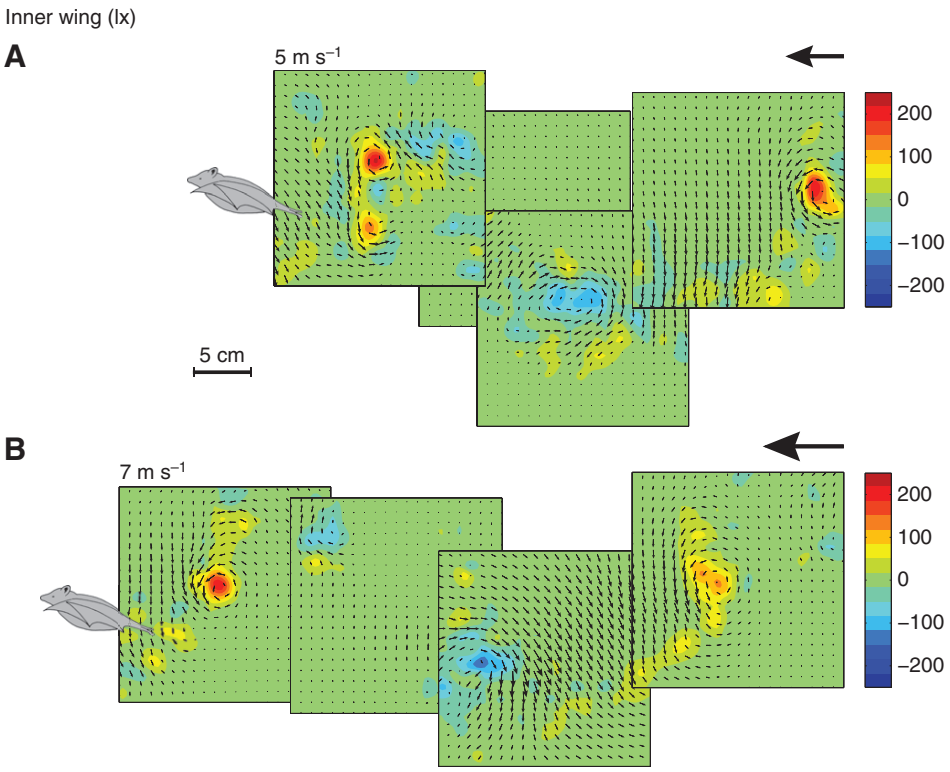

Fig. 6. Composite wake velocity and vorticity plots of the far wake in the streamwise plane [*x*, *z*] for the inner wing (lx) at flight speeds of 5 and 7 m s^{-1}. For further explanation, see Fig. 3.

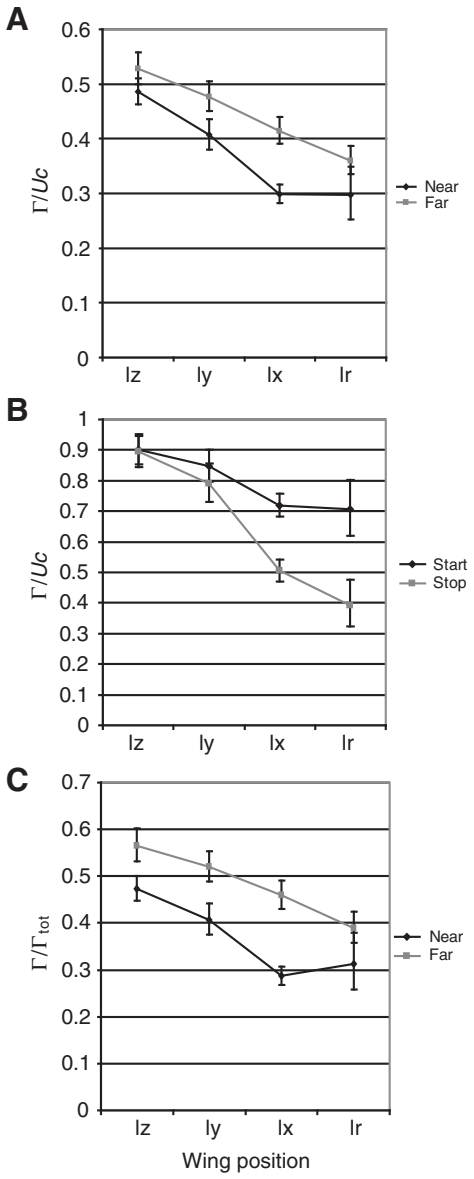

Fig. 7. Estimated marginal means from the statistical model (see text). Error bars represent the 95% confidence interval of the estimate and wing positions are outer wing (Iz), mid-wing (Iy), inner wing (Ix) and centre of body (Ir). (A) Normalized circulation Γ/Uc of the main start and stop vortices at different wing positions in the near and far wake based on the combined dataset. The means were estimated at a flight speed of U=5.3 m s^{-1}. c, mean chord. (B) Normalized circulation (Γ/Uc) of the main start and stop vortices at different wing positions based on the near-wake data. The means were estimated at U=3.5 m s^{-1}. (C) Circulation of the main start and stop vortices relative to the total circulation (Γ/Γ_{tot}) of the same sense at different wing locations in the near and far wake, based on the combined data set. The means were estimated at U=5.4 m s^{-1}.

(Fig. 4), the beginning of the downstroke was associated with an induced upwash followed by a large start vortex and then trailing patches of start vorticity (ω^+). The timing of the inner wing upwash in the stroke cycle was determined by studying the transverse plane [y, z], which showed a downwash at the end of the upstroke and an upwash at the beginning of the downstroke for the inner wing (lx) and body positions (lr). At these higher speeds of 3 to 7 m s^{-1}, the stop vortex shed at the inner wing was more diffuse than at slower speeds, and had a relatively lower circulation, Γ^-/Γ_{tot}^-. A vortex ring producing a weak upward-induced flow is known to be shed at the outer wing at the end of the upstroke (Hedenström et al., 2007), but with an associated vertical force of only 0.4% and 1% of the weight of the animal at 4 and 6.5 m s^{-1}, respectively.

Trends and patterns

The absolute value of the total circulation of start ($|\Gamma_{tot}^+|$) and stop ($|\Gamma_{tot}^-|$) vortices decreased, as did peak vorticity ($|\omega^+|$ and $|\omega^-|$) and circulation of the main start ($|\Gamma^+|$) and stop ($|\Gamma^-|$) vortices, with increasing flight speed (Table 2; see supplementary material Figs S3 and S4 for the raw data). Also, the strength of the main start vortex relative to the total circulation of the start vortices (Γ^+/Γ_{tot}^+) in the streamwise plane [x, z] did not change significantly with speed (Table 2). However, when analysing a subset of the near-wake data, we found a significant negative trend in the Γ^+/Γ_{tot}^+ for speeds >3 m s^{-1} (Table 2).

There were significant differences between the spanwise wing positions (Table 2) with a trend of decreasing strength of the main start (ω^+ and Γ^+) and stop (ω^- and Γ^-) vortices in the streamwise plane [x, z] going from the outer wing towards the centre of the body (Fig. 7B). This trend was present in both the near and the far wakes (Fig. 7A). The rate of decrease in strength from the outer wing to the centre of the body differed for the start and stop vortices, as indicated by the significant interaction between the sense of circulation and wing position, with a more pronounced trend for the stop vortex than for the start vortex (Table 2, Fig. 7). However, the total circulation of start (Γ_{tot}^+) and stop (Γ_{tot}^-) vortices in the streamwise [x, z] plane did not differ between wing positions (Table 2).

The transverse [y, z] images (Fig. 1) showed a tip vortex as well as a vortex of opposite sense at the wing root (root vortex) at all speeds studied (1.5, 4 and 6.5 m s^{-1}) throughout most of the wingbeat cycle. The ratio between the root and tip vortex strength was approximately 0.5 at the studied speeds. Only at the end of the upstroke was the root vortex absent at speeds of 4 and 6.5 m s^{-1}. At the beginning of the downstroke the 'root' vortex was not located at the wing root, but further out on the wing and it migrated towards the wing root as the stroke progressed. Wingbeat phase, as well as the interaction between tip/root and phase, were significant factors in the statistical model, showing that the peak vorticity magnitude and circulation varied over the stroke cycle and did so differently for the tip and the root vortices (Table 3).

Near-/far-wake comparison

The far wake (Figs 5 and 6) showed similar patterns to the near wake, with a few notable differences. The peak vorticity of the main start (ω^+) and stop (ω^-) vortices was lower in the far wake than in the near wake (Table 4). However, the circulation of the main start and stop vortices was higher in the far wake than in the near wake (Fig. 7A), but there was no difference in the total streamwise [x, z] start or stop circulation between the near and far wake (Table 4). Taken together, this suggests that the strength of the main start and stop vortices in the far wake was higher relative to the total circulation (Γ/Γ_{tot}) in the images. However, although there was such a trend in the data, the result was not significant (Fig. 7; Table 4). The difference between near and far wakes was most pronounced for the stop vortices shed at the inner wing (Fig. 7), where the stop vortices, which had a rather diffuse distribution in the near wake (see Fig. 4), had rolled up into a more distinct structure when reaching the far-wake position (Fig. 6). This is manifested in a significant difference in the circulation for the different wing positions between the near and far wakes, as indicated by the interaction between near/far and wing position (Table 4).

Table 2. *P*-values for analysis of the near-wake data

	$\lvert\omega\rvert c/U$	$\lvert\Gamma\rvert/Uc$	$\lvert\Gamma_{tot}\rvert/Uc$	Γ/Γ_{tot}	$\Gamma^{+}/\Gamma_{tot}^{+}$ (U>3 m s^{-1})
Intercept	**0.001**	**<0.0005**	**<0.0005**	**<0.0005**	0.188
Speed (U)	**<0.0005**	**<0.0005**	**<0.0005**	0.153	**<0.0005**
Start/Stop (SS)	**<0.0005**	**<0.0005**	0.754	**<0.0005**	–
Position (Pos.)	**<0.0005**	**<0.0005**	0.294	**0.001**	**0.043**
Bat	0.072	0.435	0.694	0.138	0.012
SS×Pos.	**<0.0005**	**<0.0005**	**0.001**	**<0.0005**	–
SS×Bat	0.616	0.477	0.403	0.696	–
Pos.×Bat	0.830	0.982	0.175	0.757	0.384

P-values in bold are significant. ω, vorticity; Γ, circulation; Γ^{+}, circulation of main start vortex in streamwise velocity fields; c, mean chord; subscript tot, total.

Individual differences

In none of the tests performed was 'Bat' or any of the interactions including 'Bat' significant (Tables 2–4), suggesting that any differences between the two individuals were small.

DISCUSSION

Far wakes miss details observable in near wake

This study allows for a comparison of wake measurements from the near and far wake of the same animal. The results show that there is a difference in the peak vorticity of the main start (ω^{+}) and stop vortices (ω^{-}), with higher values measured in the near wake than in the far wake, as expected based on simple diffusion of vorticity (e.g. Tritton, 1988). The results thus display the same trend as experimental results from fixed wing studies (Spedding et al., 2006). The total circulation in the image of start (Γ_{tot}^{+}) or stop (Γ_{tot}^{-}) vortices did not differ between the near and far wake (Table 4). This is also in line with previous studies on fixed wings (Spedding et al., 2006), and suggests that it can be informative to study far wakes, as is commonly the case when working on unrestrained live flying animals, but that not all measurements will be affected similarly. The estimates of circulation of the main start and stop vortices showed, somewhat counter-intuitively, higher values in the far wake than in the near wake. This was primarily because the rather diffuse stop vortex shed at the inner wing became more concentrated in the far wake (Fig. 7A). The merger of two like-signed vortices (e.g. Melander et al., 1988; Meunier and Lewecke, 2005) is accompanied by an increased circulation of the new merged object, compared with each of its components (the total circulation is conserved), and the increase in circulation of trailing vortices as they entrain vorticity from their surroundings has also been shown in the near wake of an oscillating wing (Birch and Lee, 2005).

The near wake is much more readily tied to the generating wing kinematics and it also contains details of vortex structures that could easily be missed in the far wake. For example, the vortex ring generated by the outer wing at the end of the upstroke was clearly visible in the near wake, and although it was also visible in the far wake (when it was known where to look) it had often been moved by convection out of the field of view. Hence, studying only the far wake may lead to an over-simplified view of the wake structure.

Table 3. *P*-values for comparison between the tip vortex and wing root vortex

	$\lvert\omega\rvert c/U$	$\lvert\Gamma\rvert/Uc$
Intercept	**<0.0005**	**<0.0005**
Speed (U)	**<0.0005**	**<0.0005**
Tip/root (TR)	**<0.0005**	**<0.0005**
Phase	**0.032**	**0.044**
Bat	–	–
TB×phase	**0.007**	**0.011**
TB×bat	0.888	0.763
Phase×bat	0.831	0.728

P-values in bold are significant. ω, vorticity; Γ, circulation; c, mean chord.

Double 'start' vortices at 2 m s^{-1}

At 2 m s^{-1} we observed a novel vortex wake (Figs 3 and 4). Here, the wake contained two consecutive vortices of start (positive sign) sense but only one stop vortex, as seen both at the inner and at the outer wing position. This wake pattern is found at a flight speed where the upstroke is almost vertical relative to still air, which based on kinematics occurs at 2–3 m s^{-1} (0.43<Strouhal number, $St=fA/U$<0.75) in this species (Lindhe Norberg and Winter, 2006). The upstroke may thus generate thrust or negative thrust, depending on the sign of circulation around the wings. However, when the upstroke is vertical, weight support should be negligible or even negative and the downstroke alone must generate full weight support. At 2.5 m s^{-1}, the wake of the two bats differed, with one displaying the characteristics of 2 m s^{-1} flight speed and the other the characteristics of 3 m s^{-1}, suggesting some variation between individuals due to small differences in movement patterns of the wings. In the absence of transverse [y, z] velocity field data at this flight speed, we cannot determine how this wake pattern connects in three dimensions or at exactly which phase of the stroke the 'start' vortices are formed. Therefore we can only speculate about the origin of the double 'start' vortices. One possibility is that it represents two phases of the build-up of the circulation around the wing, one attributed to the rotation of the wing at the end of the upstroke/beginning of the downstroke and the second attributed to the linear acceleration of the wing. A second possibility is that the second 'start' vortex represents the shedding of a trailing edge vortex built up during the first part of the downstroke. Shedding of trailing edge vortices has been observed in heaving plate experiments at high St and/or high angles of attack (e.g. Jones and Platzer, 1997; Lewin and Haj-Hariri, 2003), both criteria

Table 4. *P*-values for comparison between the near- and far-wake data

	$\lvert\omega\rvert c/U$	$\lvert\Gamma\rvert/Uc$	$\lvert\Gamma_{tot}\rvert/Uc$	Γ/Γ_{tot}
Intercept	**<0.0005**	**<0.0005**	**<0.0005**	**<0.0005**
Speed (U)	**<0.0005**	**<0.0005**	**<0.0005**	0.364
Near/far (NF)	**<0.0005**	**0.031**	0.097	0.067
Start/stop (SS)	**<0.0005**	0.089	0.063	0.088
Position (Pos.)	**0.001**	**<0.0005**	0.591	**<0.0005**
Bat	–	0.378	0.430	0.813
NF×SS	**0.013**	0.151	0.744	0.510
NF×Pos.	**0.043**	**<0.0005**	0.651	**<0.0005**
NF×Bat	0.435	0.249	0.119	0.062
SS×Pos.	**<0.0005**	**<0.0005**	0.422	**<0.0005**
SS×Bat	0.580	0.137	0.753	0.227
Pos.×Bat	0.716	0.967	0.672	0.987

P-values in bold are significant. ω, vorticity; Γ, circulation; c, mean chord; subscript tot, total.

being fulfilled by the bats at this flight speed (Hedenström et al., 2007). However, measurements directly above the wing surface in this species have shown a continuous shedding of trailing edge vorticity during the downstroke at $1\,m\,s^{-1}$ (Muijres et al., 2008) and it needs to be confirmed whether the pattern is indeed qualitatively different at $2\,m\,s^{-1}$.

Inverted rings with negative lift – control or unavoidable cost?

Kinematic studies of flying bats have provided a basis for aerodynamic hypotheses (Aldridge, 1986; Aldridge, 1987; von Helversen, 1986; Lindhe Norberg and Winter, 2006; Norberg, 1976a; Norberg, 1976b), including the prediction of negative circulation at the outer wing during the end of the upstroke (Norberg, 1976a; Norberg, 1976b). This was confirmed by Hedenström and colleagues (Hedenström et al., 2007), but not further explored in quantitative detail. In fact, the circulation around the wing during the end of the upstroke differs in sign between the inner and outer part of the wing at medium ($4\,m\,s^{-1}$) and high speeds ($6.5\,m\,s^{-1}$). Qualitatively, this means that at some position along the span a vortex core, a distinct patch of streamwise vorticity, of the same sense as a 'normal' tip vortex is being shed (blue-filled circle in Fig. 8A), while at the tip of the wing the vortex has opposite-signed circulation (orange-filled circle in Fig. 8A). Because the inner part of the wing generates a downwash, the vortex structure generated here will move downwards. At the same time the outer wing generates an upwash resulting in an upward displacement of the vortex structure generated there (Fig. 8B). This should result in the vortex shed at mid-span being separated into two vortices when moving downstream, which is what is observed in most of the images (Fig. 8C). In a minority of cases, the two vortices are still connected (similar to the blue-filled circles in Fig. 8A). Shedding of trailing vortices along the span is quite common in engineered wings as a result of changes in the pressure distribution over the wing (due to extended flaps, etc.). But in most cases these vortices are the result of changes in the magnitude of the bound circulation rather than its sign.

The fact that the inner and outer part of the wing generate forces in opposite vertical directions might have consequences for the manoeuvring performance of bats. Small spanwise variations in the location of the mid-span vortex may have large consequences for the rolling moments generated by the wing as a means to increase manoeuvrability. Alternatively, the upwash may be generated as a control manoeuvre to correct pitching moments from some other phase of the wing stroke. The ring generated at the outer wing is tilted relative to the horizontal (Fig. 2), and is generated when the wing is in a position far from the centre of mass in the pitch plane [x, z], and thus could be an efficient way of generating a pitching moment. These bats do not have a tail, which might otherwise be responsible for these control moments in birds and other bats with more pronounced tail membranes. In the end it could yet be that generating this vortex is an involuntary consequence of having membranous wings, and therefore represents a cost constraint of bat flight not necessarily shared by other flying animals with non-membranous wings. The cost, as expressed in negative vertical force, is relatively small, representing only 0.4% and 1% of the weight of the bat at the speeds studied here.

At the upper turning point of the wing stroke not only the outer part of the wing but also the inner wing and body generate upward-induced flows. This happens after the outer wing has shed its negative-lift-generating vortex ring and is starting to develop circulation for the downstroke (Fig. 4). For the inner wing the stop vortex at the end of the upstroke encircles the upward flow together with wing root cores formed mid-wing at the beginning of the downstroke by the outer wing and the start vortex of the downstroke. In other words, the upward-directed flow seen at the inner wing and body occurs during the beginning of the downstroke (see above and Fig. 4). In videos of the lateral view the tail/legs move upwards relative to the body, forming a negative geometric angle of attack and the inner wing membrane 'bulges' downwards showing a loss of lift or production of negative lift, consistent with the observed wake. Consequently the circulation around all the sections of the wing changes sign during some phase of the stroke cycle. This suggests that the circulation observed in the streamwise plane [x–z], which represents the change in circulation, is able to capture the total circulation generated during a wing beat and can be used to calculate the force balance in these bats.

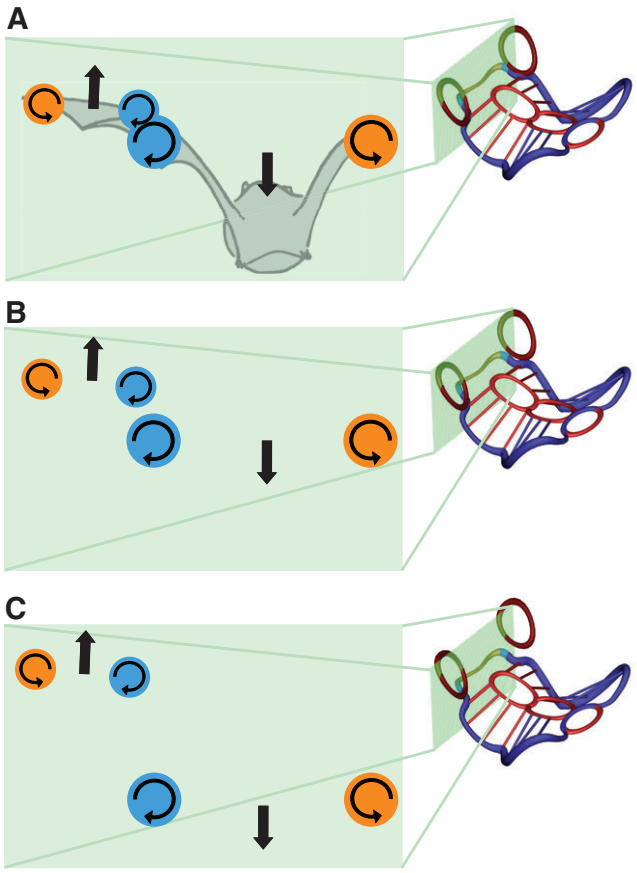

Fig. 8. Interpretation of the wake in the transverse plane [y–z] at the end of the upstroke (see text) as the wake moves progressively downstream (A–C). Inserted wake models illustrate the evolution of the wake and the cuts through the wake at the different distances downstream of the wing.

One ring or two?

At all speeds studied, each bat wing generated its own vortex loop as shown by the presence of the wing root vortices in the transverse [y, z] plane, confirming previous observations (Hedenström et al., 2007). When a wing flaps by rotation about a hinge (the wing root), there are large differences in the relative magnitude of the air flow from root to tip. At the root, the flow can be imagined to be almost steady as local vertical wing section speeds are small compared with the mean forward speed. The relative magnitude of the variation due to the flapping motion itself [and associated local section Reynolds numbers (Rosén et al., 2007)] increases towards the tip. At a local wing section the circulation will also vary in direct proportion to the local incident velocity (subject to modification from local twist, camber, flexibility and thickness) and if the bound circulation changes then so must the circulation deposited into the wake. This section-

by-section, quasi-two-dimensional concept of wing circulation makes the formation of two separate rings behind flapping wing pairs quite a likely outcome, and many such complicated wake structures have been reported in the insect flight literature (e.g. Aono et al., 2008; Brodsky, 1991; Grodnitsky and Morozov, 1993). However, the shedding and subsequent roll-up of shed vorticity is not easy to predict and may be very different from a quasi-two-dimensional process.

Here, the measured spanwise variations in wake circulation are consistent with the observation that each bat wing makes (at least) one ring of its own. Far-wake measurements of birds in similar circumstances do not show such circulation gradients and have not found significant drops in wake circulation at the centreline. However, a recent study of swift wakes shows a reduction of the induced downwash behind the body relative to that of the wings (Henningsson et al., 2008), which should be indicative of wing root vortices. There are no conclusive data from transverse planes in bird wakes, and although the existing models based on far-wake measurements of bird flight have single loops for each wing pair, it may be that higher resolution data in transverse planes and closer to the animal might show this to be an oversimplified concept.

We thank P. Henningsson for comments on parts of the manuscript. This work was supported by grants from the Swedish Research Council, the Swedish Foundation for International Cooperation in Research and Higher Education, the Knut and Alice Wallenberg Foundation, the Crafoord Foundation, the Magnus Bergvall Foundation, the Royal Physiographical Society in Lund, and the Volkswagen Stiftung. The experiments were approved by the Lund University ethical board (M153-05).

LIST OF ABBREVIATIONS

A	tip-to-tip amplitude of wing motion
AR	aspect ratio, b/c
b	wingspan
c	mean chord
d_{xz}	diameter of vortex ring at end of upstroke in streamwise plane [x–z]
d_{yz}	diameter of vortex ring at end of upstroke in transverse plane [y–z]
eu	end of upstroke
f	wingbeat frequency
F_v	vertical force generated by vortex at end of upstroke
I_{eu}	vertical impulse generated by vortex at end of upstroke
l	characteristic length
lr	mid-body position
lx	inner wing position
ly	mid-wing position
lz	outer wing position
S_{eu}	horizontally projected area of vortex at end of upstroke
T_{eu}	formation time of vortex at end of upstroke
U	flight speed and wind tunnel speed
u	velocity in streamwise direction
v	velocity in spanwise direction
w	velocity in vertical direction
x	downstream distance from trailing edge of wing to imaging area and streamwise axis
y	spanwise axis
z	vertical axis
δt	time interval between images in DPIV analysis
γ_{xz}	angle relative to horizon of vortex ring at end of upstroke in streamwise plane [x–z]
γ_{yz}	angle relative to horizon of vortex ring at end of upstroke in transverse plane [y–z]
Γ	circulation
Γ^+	circulation of main start vortex in streamwise velocity fields
Γ^-	circulation of main stop vortex in streamwise velocity fields
Γ_{eu}^-	negative circulation of vortex ring shed at end of upstroke
Γ_{tot}^+	total circulation of start sense in streamwise velocity fields
Γ_{tot}^-	total circulation of stop sense in streamwise velocity fields
ν	kinematic viscosity
ρ	air density
ω	vorticity
ω^+	peak vorticity of main start vortex in streamwise velocity fields
ω^-	peak vorticity of main stop vortex in streamwise velocity fields

REFERENCES

Aldridge, H. D. J. N. (1986). Kinematics and aerodynamics of the greater horseshoe bat, *Rhinolophus ferrumequinum*, in horizontal flight at various flight speeds. *J. Exp. Biol.* **126**, 479-497.
Aldridge, H. D. J. N. (1987). Body accelerations during the wingbeat in six bat species: the function of the upstroke in thrust generation. *J. Exp. Biol.* **130**, 275-293.
Aono, H., Liang, F. and Liu, H. (2008). Near- and far-field aerodynamics in insect hovering flight: an integrated computational study. *J. Exp. Biol.* **211**, 239-257.
Birch, D. and Lee, T. (2005). Investigation of the near-field tip vortex behind an oscillating wing. *J. Fluid Mech.* **544**, 201-241.
Brodsky, A. K. (1991). Vortex formation in the tethered flight of the peacock butterfly, *Inachis io* L. (Lepidoptera, Nymphalidae), and some aspects of insect flight evolution. *J. Exp. Biol.* **161**, 77-95.
Fincham, A. and Delerce, G. (2000). Advanced optimization of correlation imaging velocimetry algorithms. *Exp. Fluids* **29**, S13-S22.
Fincham, A. M. and Spedding, G. R. (1997). Low-cost, high resolution DPIV for measurement of turbulent fluid flow. *Exp. Fluids* **23**, 449-462.
Grafen, A. and Hails, R. (2002). *Modern Statistics for the Life Sciences*. Oxford: Oxford University Press.
Grodnitsky, D. L. and Morozov, P. P. (1993). Vortex formation during tethered flight of functionally and morphologically two-winged insects, including evolutionary considerations on insect flight. *J. Exp. Biol.* **182**, 11-40.
Hedenström, A., Rosén, M. and Spedding, G. R. (2006a). Vortex wakes generated by robins *Erithacus rubecula* during free flight in a wind tunnel. *J. R. Soc. Interface* **3**, 263-276.
Hedenström, A., van Griethuijsen, L., Rosén, M. and Spedding, G. R. (2006b). Vortex wakes of birds: Recent developments using digital particle image velocimetry a wind tunnel. *Anim. Biol.* **56**, 535-549.
Hedenström, A., Johansson, L. C., Wolf, M., von Busse, R., Winter, Y. and Spedding, G. R. (2007). Bat flight generates complex aerodynamic tracks. *Science* **316**, 894-897.
Henningsson, P., Spedding, G. R. and Hedenström, A. (2008). Vortex wake and flight kinematics of a swift in cruising flight in a wind tunnel. *J. Exp. Biol.* **211**, 717-730.
Jones, K. D. and Platzer, M. F. (1997). Numerical computation of flapping-wing propulsion and power extraction. *AIAA Paper 97-0826*.
Lewin, G. C. and Haj-Hariri, H. (2003). Modelling thrust generation of a two-dimensional heaving airfoil in a viscous flow. *J. Fluid Mech.* **492**, 339-362.
Lindhe Norberg, U. M. and Winter, Y. (2006). Wing beat kinematics of a nectar-feeding bat, *Glossophaga soricina*, flying at different flight speeds and Strouhal numbers. *J. Exp. Biol.* **209**, 3887-3897.
Melander, M. V., Zabusky, N. J. and McWilliams, M. J. (1988). Symmetric vortex merger in two dimensions: causes and conditions. *J. Fluid Mech.* **195**, 303-340.
Meunier, P. and Lewecke, T. (2005). Elliptic instability of a co-rotating vortex pair. *J. Fluid Mech.* **533**, 125-159.
Muijres, F. T., Johansson, L. C., Barfield, R., Wolf, M., Spedding, G. R. and Hedenström, A. (2008). Leading edge vortex improves lift in slow-flying bats. *Science* **319**, 1250-1253.
Norberg, U. M. (1976a). Aerodynamics, kinematics, and energetics of horizontal flapping flight in the long-eared bat *Plecotus auritus*. *J. Exp. Biol.* **65**, 179-212.
Norberg, U. M. (1976b). Aerodynamics of hovering flight in the long-eared bat *Plecotus auritus*. *J. Exp. Biol.* **65**, 459-470.
Parker, K., von Ellenrieder, K. D. and Soria, J. (2007). Morphology of forced oscillatory flow past a finite-span wing at low Reynolds number. *J. Fluid Mech.* **571**, 327-357.
Pennycuick, C. J. (1989). *Bird Flight Performance: A Practical Calculation Manual*. Oxford: Oxford University Press.
Pennycuick, C. J., Alerstam, T. and Hedenström, A. (1997). A new low-turbulence wind tunnel for bird flight experiments at Lund University, Sweden. *J. Exp. Biol.* **200**, 1441-1449.
Ramasamy, M., Lee, T. E. and Leishman, J. G. (2007). Flowfield of a rotating-wing micro air vehicle. *J. Aircr.* **44**, 1236-1244.
Rosén, M., Spedding, G. R. and Hedenström, A. (2007). Wake structure and wingbeat kinematics of a house-martin *Delichon urbica*. *J. R. Soc. Interface* **4**, 659-668.
Spedding, G. R. (2003). Comparing fluid mechanics models with experimental data. *Phil. Trans. R. Soc. Lond., B, Biol. Sci.* **358**, 1567-1576.
Spedding, G. R., Hedenström, A. and Rosén, M. (2003a). Quantitative studies of the wakes of freely-flying birds in a low-turbulence wind tunnel. *Exp. Fluids* **34**, 291-303.
Spedding, G. R., Rosén, M. and Hedenström, A. (2003b). A family of vortex wakes generated by a thrush nightingale in free flight in a wind tunnel over its entire natural range of flight speeds. *J. Exp. Biol.* **206**, 2313-2344.
Spedding, G. R., McArthur, J. and Rosén, M. (2006). Deducing aerodynamic mechanisms from near- and farwake measurements of fixed and flapping wings at moderate Reynolds number. AIAA 2006-33, *44th AIAA Aerospace Sciences Meeting and Exhibit, Reno, Nevada*.
Tian, X., Iriarte-Dias, J., Middleton, K., Galvao, R., Israeli, E., Roemer, A., Sullivan, A., Song, A., Swartz, S. and Breuer, K. (2006). Direct measurements of the kinematics and dynamics of bat flight. *Bioinspir. Biomim.* **1**, S10-S18.
Tritton, D. J. (1988). *Physical Fluid Dynamics*. New York: Oxford University Press.
von Ellenrieder, K. D., Parker, K. and Soria, J. (2003). Flow structures behind a heaving and pitching finate span wing. *J. Fluid Mech.* **490**, 129-138.
von Helversen, O. (1986). Blütenbesuch bei Blumenfledermäusen: Kinematik des Schwirrfluges und Energiebudget im Freiland. In *Biona-report* **5**, *Fledermausflug-bat flight* (ed. W. Nachtigall), pp. 107-126. Stuttgart: G. Fischer.